Computer Methods in Biomechanics and Biomedical Engineering

Publication details, including instructions for authors and subscription information:
http://www.tandfonline.com/loi/gcmb20

Characterisation and simulation of an active microvalve for glaucoma

F. Sassetti [a b], F. A. Guarnieri [a b], L. Garelli [a b] & M. A. Storti [b]

[a] Facultad de Bioingeniería, UNER, Ruta Prov. N 11 Km. 10, 3100, Oro Verde, Entre Ríos, Argentina

[b] Centro Internacional de Métodos Computacionales en Ingeniería (CIMEC), INTEC (UNL-CONICET), Güemes 3450, S3000GLN, Santa Fe, Argentina

Available online: 02 Aug 2011

To cite this article: F. Sassetti, F. A. Guarnieri, L. Garelli & M. A. Storti (2011): Characterisation and simulation of an active microvalve for glaucoma, Computer Methods in Biomechanics and Biomedical Engineering, DOI:10.1080/10255842.2011.585978

To link to this article: http://dx.doi.org/10.1080/10255842.2011.585978

Computer Methods in Biomechanics and Biomedical Engineering
iFirst article, 2011, 1–8

Taylor & Francis
Taylor & Francis Group

Characterisation and simulation of an active microvalve for glaucoma

F. Sassetti[a,b]*, F.A. Guarnieri[a,b], L. Garelli[a,b] and M.A. Storti[b]

[a]*Facultad de Bioingeniería, UNER, Ruta Prov. N 11 Km. 10, 3100, Oro Verde, Entre Ríos, Argentina;* [b]*Centro Internacional de Métodos Computacionales en Ingeniería (CIMEC), INTEC (UNL-CONICET), Güemes 3450, S3000GLN Santa Fe, Argentina*

(*Received 22 March 2011; final version received 3 May 2011*)

Glaucoma drainage device (GDD) has the potential to eliminate hypotony but still suffers from poor flow control and fibrosis. The ideal shunt should change its hydraulic resistance to achieve the desired intraocular pressure (IOP). In this study, the characterisation of a preliminary design of a new GDD is presented. This is activated by means of a diaphragm, which is actuated by conducting polymers. The valve can be manufactured employing microelectromechanical system technology by soft lithography. The characterisation process is performed by numerical simulation using the finite element method, considering the coupling between the fluid and the structure (diaphragm) obtaining the hydraulic resistance for several positions of the diaphragm. To analyse the hydraulic system of the microvalve implanted in a human eye, an equivalent circuit model was used. The parameters of the equivalent circuit model were obtained from numerical simulation. The hydraulic resistance of the designed GDD varies in the range of 13.08–0.36 mmHg min/μl compared with 3.38–0.43 mmHg min/μl for the Ahmed valve. The maximum displacement of the diaphragm in the vertical direction is 18.9 μm, and the strain in the plane is 2%. The proposed preliminary design allows to control the IOP by varying the hydraulic resistance in a greater range than the existing passive valves, and the numerical simulation facilitates the characterisation and the improvement of the design before its construction, reducing time and costs.

Keywords: glaucoma; glaucoma drainage device; finite element method

1. Introduction

Glaucoma is the optic nerve damage often associated with an increased intraocular pressure (IOP) that leads to progressive and irreversible loss of vision. The aqueous humour (AH) is produced in the ciliary body behind the iris (in the posterior chamber), passes into the front of the eye (anterior chamber) and then exits through the drainage channels (Figure 1). The AH leaves the anterior chamber primarily via the trabecular meshwork, and it moves exteriorly into the canal of Schlemm to the aqueous veins and then to the episcleral veins (Jacobs 2009).

The IOP for general population is in the range of 15.50 ± 2.60 mmHg (Ethier et al. 2004). Ocular hypertension is defined when the IOP is higher than 20 mmHg in the absence of optic nerve damage or visual field loss, and is the most important risk factor for glaucoma. The treatment of glaucoma consists of topical or systemic IOP lowering agents or laser treatment. When these treatments are not effective, surgery is required and more complex cases require an implant of an aqueous shunt or glaucoma drainage device (GDD).

The shunts came into use in the early 1900s, when M. Rollet implanted a horse hair connecting the anterior chamber to the subconjunctival space near the limbus. In 1969, Molteno introduced an external subconjuntival plate at the end of the tube shunt. This device and the others that are similarly used for AH drainage do not offer enough hydraulic resistance, and they can originate complications related with the hypotony in the post-operative period. To reduce the effects of hypotony, a flow resistor was added, such as the Ahmed glaucoma valve® (AGV). Another cause of failure of implants is associated with an increase in the IOP caused by the tissue–implant reaction (Hong et al. 2005). To avoid or diminish these problems, several modifications have been tried, such as increasing plate area, substituting structural materials (Ishida et al. 2006) or inserting bypass resistances with microtubes (Pan et al. 2006).

There have been attempts to replace the passive valves by active microvalves using electrochemical (Neagu 1998; Pan et al. 2007) or electromagnetic actuators (Byunghoon 2003), but several questions arise about biocompatibility and size issues.

In the patent of Guarnieri (2007) is described an active implantable microvalve. The mechanism of the microvalve includes a diaphragm made of a conjugated polymer (CP) that shows high deformation and the volume of which depends on the electric potential applied to a pair of electrodes.

In recent years, several methodologies have been proposed to simulate and characterise passive or active

*Corresponding author. Email: f_sassetti@hotmail.com

ISSN 1025-5842 print/ISSN 1476-8259 online

DOI: 10.1080/10255842.2011.585978
http://www.informaworld.com

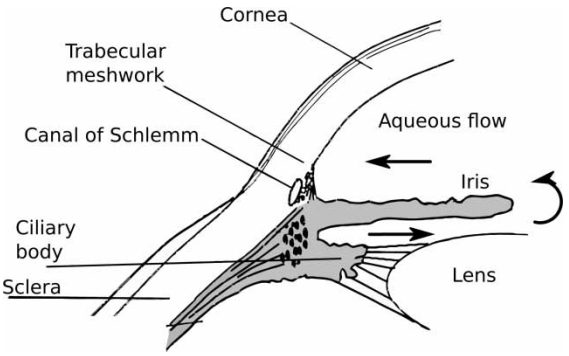

Figure 1. Aqueous humour formation and circulation. Figure adapted from Humayun et al. (2007).

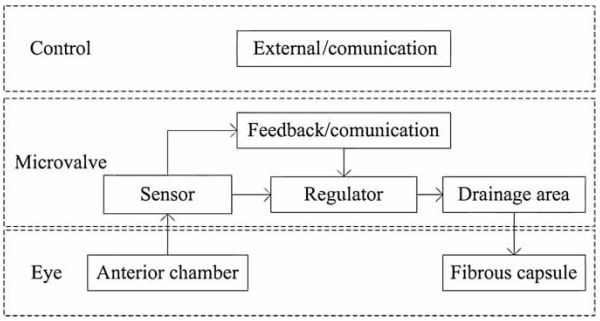

Figure 2. Schematic diagram of an active valve for glaucoma treatment.

drainage devices (Neagu 1998). In the study of Pan et al. (2003), two uncoupled models are used to characterise the AGV. First, the leaf displacement is obtained applying an evenly distributed pressure. Then, from the structural results, the geometry and the boundary conditions are established for the fluidic analysis. This is the simplest way to consider certain structural aspects on the fluid dynamics of the valve. A more complex model is presented by Stay et al. (2005), in which the leaves of the AGV were modelled using the Von Karman plate theory, coupled to a Reynolds lubrication theory model of the AH flow through the valve, resulting in a 2D-coupled partial differential equation. In this model, the governing equation is coupled in a monolithic way and presents some advantages over the modelling done by Pan et al. (2003), because the pressure distribution is given by the fluid dynamics of the problem. But one limitation is the inherent 2D geometry of the fluid domain to be simulated.

In this paper, the characterisation and simulation of the active microvalve proposed in Guarnieri (2007) are presented for the treatment of glaucoma. The performance of the microvalve is evaluated using tools from the computational mechanics and a circuit equivalent model.

2. Materials and methods

2.1 Active microvalve

In Figure 2, a schematic diagram and the components that comprise the active valve are shown. The regulator was designed to control the IOP by varying its resistance to the AH flow, by means of the deflection of the diaphragm. The regulator is conceptually a normally closed valve, with a small leakage flow.

The hydraulic resistance of the regulator has a passive component due to the effects of fluid pressure on the diaphragm and an active component due to the change in the geometry. When a voltage difference in the range of 1–2 V is applied between the actuators' face, a deformation in the plane of the CPs in the range of 1–3% of its initial dimensions is produced (Smela 1999). The deformation generates the bending of the diaphragm, decreasing the hydraulic resistance between the input and output channels.

In Figure 3, a cross section of the geometry of the regulator is shown. The channels (inlet and outlet) are connected by a deformable chamber. The valve structure is made of medical grade silicone (Nusil Med-6215). The use of these materials allows the regulator to be manufactured using soft lithography.

The actuator has a thickness of 30 μm, and is composed mainly of a CP electrochemically deposited on a thin film conductor. The rigidity of the diaphragm is given by the properties of CP with Young's modulus of 450 MPa, which is greater than 0.75 MPa of the silicone and Poisson's ratios are 0.3 and 0.5, respectively.

2.2 Numerical model and simulation

In this work, a fully coupled 3D model is used. The AH is described by the incompressible Navier–Stokes equations, written in an arbitrary time-dependent coordinate system. Equation (1) expresses the conservation of mass for incompressible fluids and Equation (2) the conservation of momentum:

$$\nabla\cdot\mathbf{v} = 0, \tag{1}$$

$$\rho\frac{\partial\mathbf{v}}{\partial t} + \rho[(\mathbf{v} - \mathbf{v}_{\mathrm{m}})\cdot\nabla]\mathbf{v} = \nabla\cdot\boldsymbol{\sigma}, \tag{2}$$

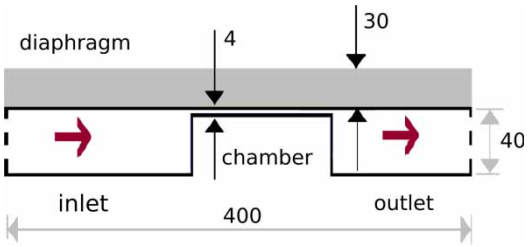

Figure 3. Geometry of the regulator.

where $\mathbf{v}$ is the fluid velocity, ρ is the density, $\mathbf{v}_m$ is the velocity of the moving reference frame and $\boldsymbol{\sigma}$ is the stress tensor (pressure and viscous forces). Assuming that the fluid is Newtonian, its constitutive equation is given by

$$\boldsymbol{\sigma} = \tau - p\mathbf{I} \text{ with } \tau = \mu[\nabla\mathbf{v} + (\nabla\mathbf{v})^{\mathrm{T}}], \tag{3}$$

where μ is the dynamic viscosity and p is the fluid pressure. To close the flow equations, a set of boundary conditions are imposed

$$\boldsymbol{\sigma}\cdot\mathbf{n} = \bar{\mathbf{t}} \text{ on } \Gamma_N, \quad \mathbf{v} = \bar{\boldsymbol{\nu}} \text{ on } \Gamma_D, \tag{4}$$

where Γ_N is a Neumann condition in the form of prescribed surface forces (tractions) and Γ_D is a Dirichlet condition where the velocity is imposed. For the structure, a constitutive linear elastic solid assuming large displacements and rotations is adopted. The structure is described by the displacement vector $\mathbf{u}$, the velocity field $\mathbf{v}_s = \partial\mathbf{u}/\partial t$, the density of the material $\boldsymbol{\rho}_s$ and the Cauchy stress tensor σ_s. Written in a Lagrangian description, with respect to the initial state Ω_s, we have

$$\rho_s \frac{\partial^2\mathbf{u}}{\partial t^2} = \nabla\cdot\mathbf{P} \text{ in } \Omega_s, \tag{5}$$

where the tensor $\mathbf{P} = J\boldsymbol{\sigma}_s\mathbf{F}^{\mathrm{T}}$ is called the first Piola–Kirchhoff tensor and $\mathbf{F} = \mathbf{I} + \nabla u$. For a convenient specification of the constitutive equation, the second Piola–Kirchhoff stress tensor $\mathbf{S}$ is introduced, and it is related to the first Piola–Kirchhoff stress tensor by $\mathbf{S} = \mathbf{F}^{-1}\mathbf{P}$. For an isotropic linear elastic material, the constitutive equation can be stated as

$$\mathbf{S} = \lambda(\mathrm{tr}\,\mathbf{E})\mathbf{I} + 2\mu\mathbf{E}, \tag{6}$$

which relates the second Piola–Kirchhoff stress tensor with the Green–Lagrange strain tensor $\mathbf{E}$ by means of the Lamé constants λ and μ. The Green–Lagrange strain tensor is defined as

$$\mathbf{E} = \frac{1}{2}(\nabla\mathbf{u} + \nabla\mathbf{u}^{\mathrm{T}} + \nabla\mathbf{u}\cdot\nabla\mathbf{u}^{\mathrm{T}}). \tag{7}$$

The coupling of these governing equations is carried out using a partitioned algorithm via fixed point iteration. For the fluid problem, an arbitrary Lagrangian–Eulerian formulation is used to define a reference system following the moving boundaries while the structure is deformed.

The partitioned algorithm and the governing equations are implemented in the portable extensible toolkit for scientific computations-finite element method (PETSc-FEM) code (Storti et al.), which is a parallel multiphysics finite element program based on the message passing interface) and the PETSc library (Balay et al.). The basic scheme for the fluid-structure interaction (FSI) considered in this work proceeds as follows:

(1) transferring the motion of the wet boundary of the solid to the fluid problem;
(2) updating the position of the fluid boundary and the bulk fluid mesh accordingly;
(3) advancing the fluid system and computing new pressures;
(4) converting the new fluid pressure (and stress field) into the structural load;
(5) advancing the structural system under the flow loads.

In this algorithm, three codes CFD (computational fluid dynamics), CSD (computational structure dynamics) and CMD (computational mesh dynamics) are running simultaneously. A schematic diagram is shown in Figure 4.

At time $\mathbf{t}_n$, we define $\mathbf{w}^n$ to be the fluid state vector $(\rho, \mathbf{v}, p)$, $\mathbf{u}^n$ the displacement vector (structure state vector) and $\mathbf{X}^n$ the fluid mesh node positions. A more detailed description about the implementations of this coupling strategy can be viewed in Storti et al. (2009) and Garelli et al. (2010).

This methodology allows to simulate both active and passive valves that have inherently 3D flows. In the case of

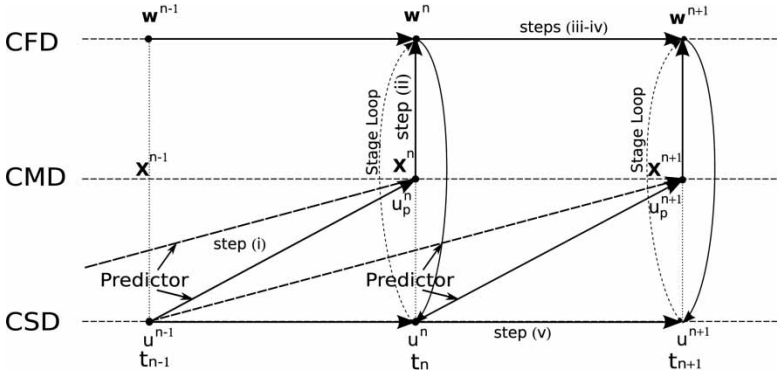

Figure 4. Synchronous FSI partitioned scheme.

passive valves, the fluid pressure deforms the diaphragm changing the hydraulic resistance; and in the case of active valves, the diaphragm deformation is prescribed as the time function, changing the hydraulic resistance.

The PETSc-FEM code has been previously used in the resolution of problems in microfluidics and electrokinetic flows (Kler et al. 2009, 2010). Therefore, to validate the proposed coupling algorithm, the AGV is simulated with the geometry and mechanical properties described in Stay et al. (2005).

Only half of the AGV geometry was simulated due to its symmetrical nature, reducing the size of the discrete problem. The valve is discretised using a structured mesh with 37,500 linear hexahedral elements for the fluid and 15,000 linear hexahedral elements for the structure. The problem was solved for several pressure drops through the valve to construct a flow rate curve.

Then, the characterisation process of the active microvalve is carried out in two stages. In the first stage, the passive resistance of the microvalve is obtained. In the second stage, the active resistance of the microvalve is analysed, this is when the diaphragm is actuated. In this case, the diaphragm is deformed and the hydraulic resistance is decreased due to a change in the geometry of the chamber.

To carry out this simulation, the microvalve was discretised using a structured mesh with 147,920 linear hexahedral elements for the fluid and 137,388 linear hexahedral elements for the structure. Only half of the structure mesh is shown in Figure 5 to obtain a clear view of the fluid mesh.

To determine the variation in the passive hydraulic resistance of the microvalve due to fluid pressure over the diaphragm, the flow rates were measured for different pressure drops. The outlet pressure was set at 8 mmHg, and the entry ranged from 15 to 60 mmHg. For each case, the flow rate and the maximum displacement of the diaphragm were obtained. The active hydraulic resistance was calculated by setting a pressure drop of 7 mmHg in the microvalve, varying the position of the diaphragm due to a deformation of the CP.

The numerical problem was carried out on a Beowulf cluster machine using 30 processors Intel® Pentium IV® Prescott 3 GHz with 2 GB of RAM, interconnected with two switch Gigabit Ethernet (1 Gbit/s), 3Com® Super Stack 3.

2.3 *Equivalent circuit model*

To analyse the hydraulic system of the microvalve implanted in a human eye, an equivalent circuit model was used, which is shown in Figure 6 as proposed by Pan et al. (2006). The circuit incorporates the effects of venous pressure and hydraulic resistance of the fibrous capsule that forms after the valve is implanted. The current source represents the generation of AH (2.5 μl/min) from the ciliary body of the eye; the capacitor depicts the capacity of the anterior chamber. Finally, the drainage is achieved on the episcleral vein at a pressure between 8 and 10 mmHg (Weinreb et al. 2007). The resistances of the model are represented by the hydraulic resistance of the microvalve (R_H) and the natural pathways of the eye (trabecular meshwork and uveoscleral outflow) (R_{OF}).

In Table 1, the parameters used in the equivalent circuit are described.

The value of the I_{OP} is obtained for a steady state condition. This steady state is obtained when the flow entering the anterior chamber is equal to the output flow and remains constant.

The AH passes through the hydraulic resistance to reach the drain. This resistance is calculated using Equation (8), where the R_H is obtained from the FEM simulation and the R_{OF} is in the range of 10–100 mmHg min/μl (Freddo and Johnson 2008):

$$R_{EQ} = \frac{R_H \times R_{OF}}{R_H + R_{OF}}. \tag{8}$$

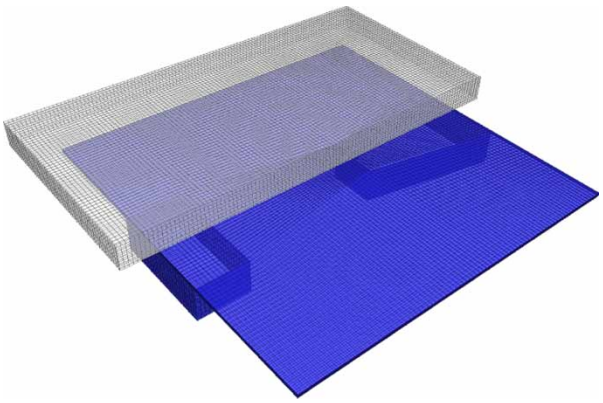

Figure 5. Structured mesh of the proposed microvalve.

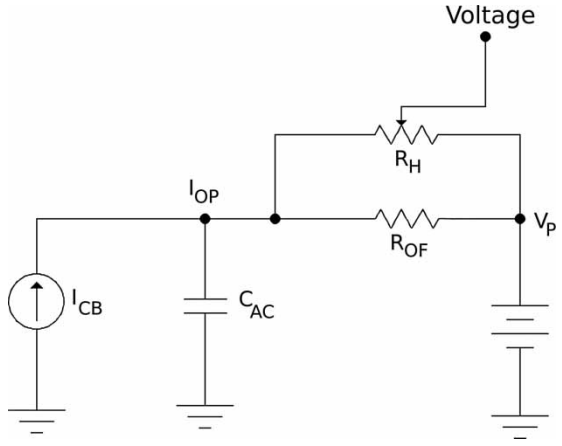

Figure 6. Equivalent circuit model.

Table 1. Equivalent circuit model parameters.

Parameters	Description	Value
I_{OP}	IOP	15 mmHg
I_{CB}	Flow ciliar body	2.5 μl/min
C_{AC}	Capacitor anterior chamber	–
V_P	Venous pressure	8 mmHg
R_{OF}	Outflow resistance	10–100 mmHg min/μl
R_H	Microvalve resistance	Variable

With the value of the equivalent hydraulic resistance, the IOP was calculated using Equation (9), where V_P is the venous pressure and q is the flow of AH:

$$I_{OP} = V_P + R_{EQ} \times q. \quad (9)$$

3. Results

In this section, the results of the validation test and the characterisation of the microvalve are shown. First, the passive hydraulic resistance is computed and then, the active hydraulic resistance. The equivalent circuit model is constructed using the obtained data from the previous simulations.

3.1 Validation test

The results of the validation test proposed in Section 2.2 are presented. Table 2 shows the flow rate obtained by Stay et al. (2005) and Kara and Kutlar (2010) for AGV and they are compared with the results of PETSc-FEM.

The wall time to obtain a steady-state solution was around 20 min using 30 processors Intel® Pentium IV® Prescott 3 GHz**.** In the range of normal operation of the valve, the flow rate is similar to that obtained by Stay et al. (2005) in their experiments.

3.2 Passive hydraulic resistance

In this section and the following, the results of the characterisation process of the microvalve are presented. Table 3 shows the flow rates for different pressure drops, and it was concluded that the designed microvalve does not work as a passive pressure regulator, as the hydraulic resistance does not decrease with increasing IOP. The wall time to obtain the equilibrium state between pressure and elastic forces was around 25 min using 30 processors.

Table 3. Passive hydraulic resistance.

IOP (mmHg)	Displacement (μm)	Flow (μl/min)	Resistance (mmHg min/μl)
15.00	0.024	0.54	13.08
22.50	0.049	1.12	12.96
30.00	0.074	1.72	12.80
37.50	0.100	2.32	12.72
45.00	0.125	2.94	12.59
52.50	0.151	3.56	12.50
60.00	0.176	4.20	12.38

In Figure 7, the pressure distribution is plotted along with the velocity field in the centre plane of the microvalve for a pressure drop of 52 mmHg.

3.3 Active hydraulic resistance

As was mentioned before, the application of a voltage to the actuator deforms the diaphragm. This deformation reduces the hydraulic resistance of the microvalve by increasing the area of passage between the input and output channels.

To characterise the change in the hydraulic resistance, the flow rate through the valve has been measured for a set of diaphragm deformations, fixing the pressure drop to 7 mmHg. The wall time to reach the steady state was around 20 min using 30 processors.

In Table 4, the changes in the hydraulic resistance as a function of actuator deformation are shown. These results are used in Section 3.4 to obtain the IOP for different values of the hydraulic resistance of the regulator when episcleral pressure is 8 mmHg and the AH flow varies from 1 to 5 μl/min.

The hydraulic resistance of the valve varies from 13.08 to 0.36 mmHg min/μl, and the displacement of the diaphragm was in the range of 0–18.90 μm. In Figure 8, the streamlines for the maximum displacement of the

Table 2. Hydraulic resistance of AGV®.

Experimental		Stay et al.		Kara and Kutlar		PETSc-FEM	
Pressure (mmHg)	Flow rate (μl/min)	Pressure (mmHg)	Flow rate (μl/min)	Pressure (mmHg)	Flow rate (μl/min)	Pressure (mmHg)	Flow rate (μl/min)
5.20	1.54	5.80	1.55	5.37	1.6	5.80	1.90
7.40	2.51	6.52	2.51	7.74	2.5	7.01	3.81
8.51	4.95	7.71	4.96	8.51	5	8.00	5.87
9.70	9.97	9.21	9.98	9.25	10	9.00	8.71
10.50	19.95	11.02	19.96	11.29	20	11.00	17.80
10.81	24.91	11.64	24.98	11.82	25	11.50	20.00

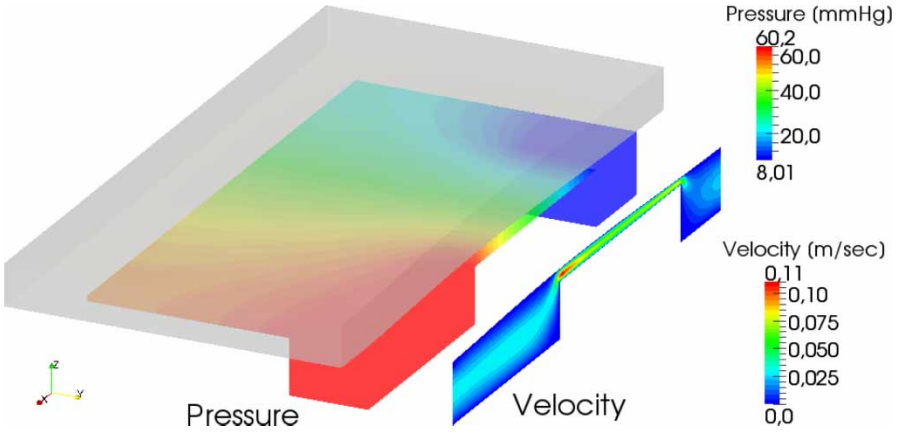

Figure 7. Pressure distribution and velocity field in the centre plane for a pressure drop of 52 mmHg.

Table 4. Active hydraulic resistance.

Deformation actuator (%)	Displacement (μm)	Aqueous flow (μl/min)	Resistance (mmHg min/μl)
0.00	0.024	0.54	13.08
0.30	2.67	1.34	5.22
0.40	3.57	1.73	4.05
0.50	4.50	2.19	3.20
1.00	9.32	5.80	1.21
2.00	18.90	19.44	0.36

diaphragm are shown, and in Figure 9, the pressure distribution is plotted along with the velocity field in the centre plane of the microvalve.

3.4 *Equivalent circuit model*

To analyse the hydraulic system of the microvalve, an equivalent circuit model was used. In Table 5, the possible values of the equivalent hydraulic resistance are presented. It was calculated for the three cases of outflow resistance ($R_{OF} = 10, 50, 100$). The different combinations between R_{OF} and R_H can give an equivalent resistance in the physiological range of 3.2–6.7 mmHg min/μl as noted by Brubaker (1998).

Figure 10 shows the values of IOP for different values of the hydraulic resistance of the regulator when episcleral pressure is 8 mmHg and the AH flow varies from 1 to 5 μl/min. The changes in the resistance of the regulator allow to control the IOP in a wide range, considering the flow rates in a physiological range.

4. Discussion

The characterised and simulated microvalve varies the hydraulic resistance by means of the deformation of a conductive polymer allowing the required control of IOP and reducing the fluctuations due to fluid–structure interaction. The proposed regulation mechanism maintains a flow of AH similar to that of a healthy eye. The design has the advantage to change the hydraulic resistance and to adapt during the fibrous tissue encapsulation process, which often leads to an increase in IOP as in the AGV®.

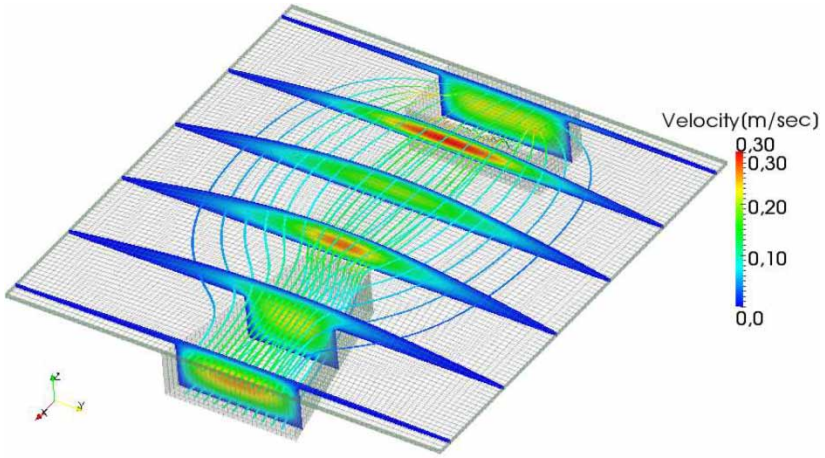

Figure 8. Streamlines for the maximum displacement of the diaphragm.

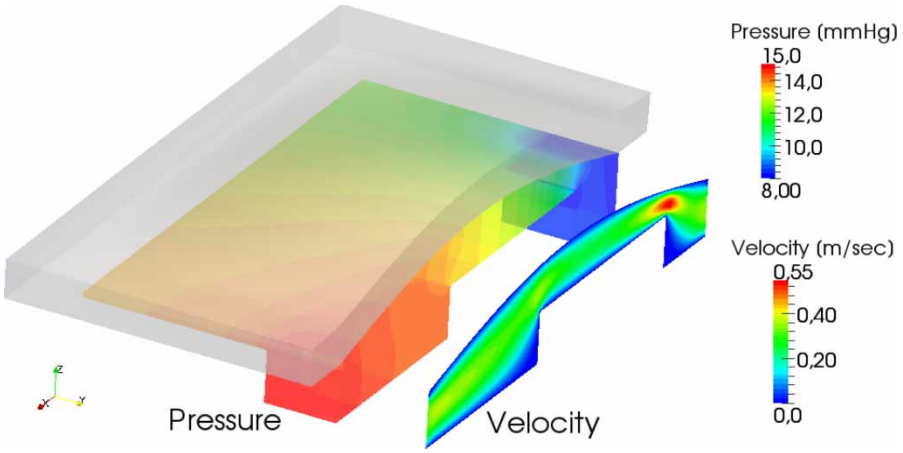

Figure 9. Pressure distribution and velocity field in the centre plane for the maximum displacement.

Table 5. Equivalent resistance.

	R_{OF} (mmHg min/μl)		
R_H (mmHg min/μl)	10	50	100
13.08	5.68	10.40	11.61
5.22	3.43	4.73	6.16
4.05	2.88	3.75	4.19
3.20	2.42	3.01	3.18
1.21	1.08	1.18	2.56
0.36	0.35	0.36	2.14

The microvalve has a passive hydraulic resistance of 13.08 mmHg min/μl, which is greater than the 3.38 mmHg min/μl of the AGV® valve for flow rates around 2 μl/min. A passive resistance of 13.08 mmHg min/μl prevents the risk of hypotony in the anterior chamber in the early stage of implantation, even when the flow of AH as low as 1 μl/min, the IOP resulting is 18.40 mmHg. The dimensions of the actuator and the proposed regulator can withstand IOP around 60 mmHg without changing the passive resistance. The proposed design would improve the control of IOP in patient's eyes with different degrees of glaucoma (10–100 mmHg min/μl) and could regulate the IOP to the target in different situations in which the flow may vary from 1 to 5 μl/min during the day.

The use of FEM allows the modelling and analysis of fluid–structure interaction of complex 3D geometries that would be difficult to resolve otherwise, enabling the improvement of the design before its construction, reducing time and costs. It also facilitates the calculation of active and passive resistance of the regulator to incorporate in the equivalent circuit model. The parallel computation

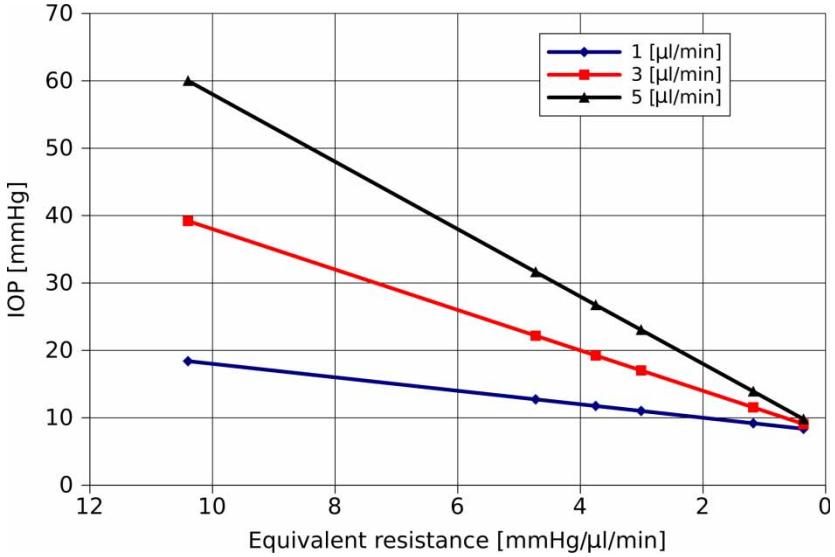

Figure 10. Intraocular pressure. $R_{OF} = 50$.

allows to compute the problem efficiently, reducing dramatically the calculus time (from day to minutes).

The coupling algorithm used in this study, in contrast with that used by Kara and Kutlar (2010), takes into account the mechanical properties of the elastomer and the geometric changes of the valve during the deformation process. The FSI scheme allows to solve the problem using both weak and strong couplings. In this study, the flow characteristics and the stiffness of the membrane make it sufficient to use a weak coupling strategy, without instability problems.

The equivalent circuit has allowed us to simulate the designed regulator and its interaction with the ocular hydraulic system.

Acknowledgements

This work has received financial support from the Consejo Nacional de Investigaciones Científicas y Técnicas (CONICET, Argentina). In this work has been extensively used the freely distributed software such as GNU/Linux OS, MPICH, PETSc, Octave, ParaView.

References

Balay S, Brown J, Buschelman K, Gropp WD, Kaushik D, Knepley MG, McInnes LC, Smith BF, Zhang H, Available from: http://www.mcs.anl.gov/petsc.

Brubaker RF. 1998. Clinical measurement of aqueous dynamics: implications for addressing glaucoma. In: Civan MM, editor. Eyes aqueous humor: from secretion to glaucoma. Current topics in membranes. Vol. 45. San Diego, CA: Academic Press. p. 233–284.

Byunghoon B. 2003. *In vitro* experiment of the pressure regulating valve for a glaucoma implant. J Micromech Microeng. 13:613–619.

Ethier CR, Johnson M, Ruberti J. 2004. Ocular biomechanics and biotransport. Annu Rev Biomed Eng. 6:249–273.

Freddo TF, Johnson M. 2008. Aqueous humor outflow resistance. In: Civan MM, editor. Eyes aqueous humor. Current topics in membranes. 2nd ed. Vol. 62, San Diego, CA: Academic Press. p. 161–192.

Garelli L, Paz RR, Storti MA. 2010. Fluid-structure interaction study of the start-up of a rocket engine nozzle. Comput Fluids. 39(7):1208–1218.

Guarnieri FA. 2007. Implantable ocular microapparatus to ameliorate glaucoma or an ocular overpressure causing disease. Available from: http://www.wipo.int/pctdb/en/wo.jsp?WO=2008084350.

Hong CH, Arosemena A, Zurakowski D, Ayyala RS. 2005. Glaucoma drainage devices: a systematic literature review and current controversies. Surv Ophthalmol. 50(1):28–60.

Humayun MS, Weiland JD, Chader G, Greenbaum E, editors. 2007. Artificial sight: basic research, biomedical engineering, and clinical advances. New York: Springer.

Ishida K, Netland PA, Costa VP, Shiroma L, Khan B, Ike I, Ahmed K. 2006. Comparison of polypropylene and silicone Ahmed glaucoma valves. Ophthalmology. 113:1320–1326.

Jacobs MD. 2009. Multiscale systems integration in the eye. Wiley Interdiscip Rev Syst Biol Med. 1:15–27.

Kara E, Kutlar AI. 2010. CFD analysis of the Ahmed glaucoma valve and design of an alternative device. Comput Methods Biomech Biomed Eng. 13(6):655–662.

Kler PA, Berli C, Guarnieri FA. 2010. Modeling and high performance simulation of electrophoretic techniques in microfluidic chips. Microfluid Nanofluid. 10(1):187–198.

Kler PA, López EJ, Dalcín LD, Guarnieri FA, Storti MA. 2009. High performance simulations of electrokinetic flow and transport in microfluidic chips. Comput Methods Appl Mech Eng. 198(30–32):2360–2367.

Neagu CR. 1998. A medical microactuator based on an electrochemical principle Universiteit Twente – Elektrotechniek. Available from: http://doc.utwente.nl/13878/.

Nusil, Med-6215 Product Profile (2008). Available from: http://www.nusil.com/library/products/MED-6215P.pdf.

Pan T, Baldi A, Ziaie B. 2007. Remotely adjustable check-valves with an electrochemical release mechanism for implantable biomedical Microsystems. Birck Nanotechnology Center Nanotechnology, Publications Purdue Libraries.

Pan T, Li Z, Brown JD, Ziaie B. 2003. Microfluidic characterization of a valved glaucoma drainage device with implications for enhanced therapeutic efficacy. Engineering in Medicine and Biology Society. Proceedings of the 25th Annual International Conference of the IEEE, Vol. 4. p. 3317–3320.

Pan T, Stay MS, Barocas VH, Brown JD, Ziai B. 2006. Modeling and characterization of a valved glaucoma drainage device with implications for enhanced therapeutic efficacy. IEEE Trans Biomed Eng. 52:948–951.

Smela E. 1999. Microfabrication of PPy microactuators and other conjugated polymer devices. J Micromech Microeng. 9:1–18.

Stay MS, Pan T, Brownb JD, Ziaie B, Barocas VH. 2005. Thin-film coupled fluid-solid analysis of flow through the Ahmed glaucoma drainage device. J Biomech Eng. 127(5):776–781.

Storti MA, Nigro N, Paz RR, Dalcin LD. 2009. Strong coupling strategy for fluid structure interaction problems in supersonic regime via fixed point iteration. J Sound Vib. 30:859–877.

Storti MA, Nigro N, Paz RR, Dalcin L, Lopez E. PETSc-FEM: a general purpose, parallel, multi-physics FEM program. Available from: http://www.cimec.org.ar/twiki/bin/view/Cimec/PETScFEM.

Weinreb RN, Brandt JD, Garway-Heath D, Medeiros FA. 2007. Intraocular Pressure. Amsterdam, The Netherlands: World Glaucoma Association.